J. Fluid Mech. (1997), *vol.* 348, *pp.* 295–317. Printed in the United Kingdom

Accelerated scalar dissipation in a vortex

By P. FLOHR AND J. C. VASSILICOS

Department of Applied Mathematics and Theoretical Physics,
University of Cambridge, Cambridge CB3 9EW, UK

(Received 17 January 1997 and in revised form 29 May 1997)

A scalar patch forms spiral structure when it wraps around an isolated vortex. It is shown that this wind-up process leads to accelerated diffusion during a time range $T_S < t < T_D$. The lower limit T_S is the time needed to create a well-defined spiral, and the upper limit T_D is the diffusive time scale of the scalar field θ in the vortex. Whereas the scaling $T_D \sim Pe^{1/3}$ is independent of the particular spiral topology, the accelerated decay of the scalar variance $\overline{\theta^2}(t)$ for earlier times is directly linked to the space-filling property of the spiral and is found to scale as $\overline{\theta^2}(0) - \overline{\theta^2}(t) \sim (Pe^{-1/3}t)^{3(1-D'_K)}$. D'_K is the Kolmogorov capacity of the spiral; it is defined in the range $1/2 < D'_K < 1$ and it is the most suitable measure of the spiral's space-filling property.

1. Introduction

A pivotal assumption in turbulence theory is the asymptotic independence of dissipation rates from diffusive properties at the molecular level. The rate of kinetic energy dissipation ϵ is usually assumed to be independent of the kinematic viscosity ν in the limit where $\nu \to 0$. Likewise, the rate of scalar dissipation χ is often assumed to be independent of molecular diffusivity κ in the limit where $\kappa \to 0$. Kolmogorov's dimensional analysis is indeed based on the assumption that $\partial\epsilon/\partial\nu = 0$ as $\nu \to 0$ and leads to $E(k) \sim k^{-5/3}$ where $E(k)$ is the energy spectrum of a homogeneous and isotropic turbulent velocity field. A similar dimensional analysis that is based on $\partial\chi/\partial\kappa = 0$ as $\kappa \to 0$ and $\partial\chi/\partial\nu = 0$ as $\nu \to 0$ leads to $\Gamma(k) \sim k^{-5/3}$ where $\Gamma(k)$ is the power spectrum of a homogeneous and isotropic turbulent scalar field (Batchelor 1959). Hunt & Vassilicos (1991) pointed out that there must be singularities in a field with a k^{-p} power spectrum and that if $p < 2$ these singularities are either isolated cusp singularities, isolated oscillating singularities or non-isolated singularities (see figure 1*a*). More precisely they must be 'near singularities', that is, they exhibit the asymptotic structure of a singularity outside a limited region where viscosity or diffusivity smooths out the field. In this paper we study the effect on scalar dissipation of a scalar isolated oscillating singularity generated by the winding action of a two-dimensional vortex. Let us now motivate this study.

A scalar field $\theta(\boldsymbol{x}, t)$ subjected to the sole action of molecular diffusion evolves according to

$$\frac{\partial}{\partial t}\theta = \kappa\nabla^2\theta. \tag{1.1}$$

An initial scalar field $\theta(\boldsymbol{x}, t = 0)$ with a k^{-p} high-wavenumber power spectrum decays faster with time for smaller values of p (Vassilicos 1995). For example, a one-dimensional initial on–off scalar function $\theta(x, 0)$ with a k^{-p} high-wavenumber

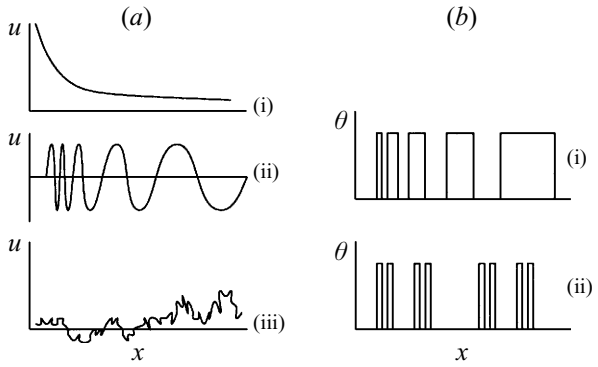

FIGURE 1. Classification of possible singular flow topology in schematic one-dimensional distributions. (*a*) A continuous field $u(x)$ can have (i) isolated cusps, (ii) isolated oscillating singularities, or (iii) non-isolated singularities as in fractal fields. (*b*) A scalar on–off field $\theta(x)$ can have (i) isolated accumulations of discontinuities which are the on–off equivalent of isolated oscillating singularities, or (ii) non-isolated fractal accumulations of discontinuities.

power spectrum and $1 < p \leqslant 2$ decays in such a way that

$$\frac{\overline{\theta^2}(0) - \overline{\theta^2}(t)}{\overline{\theta^2}(0)} \sim \left(\frac{2\kappa t}{L^2}\right)^{(p-1)/2} + O\left(\frac{\kappa t}{L^2}\right) \tag{1.2}$$

for short times $\kappa t/L^2 \ll 1$, where L is an outer length scale of the initial field and $\overline{\theta^2}(t) = (1/L)\int \frac{1}{2}|\theta(x,t)|^2 \mathrm{d}x$.

As discussed by Hunt & Vassilicos (1991), isolated discontinuities have a k^{-2} high-wavenumber power spectrum; but on–off functions $\theta(x,0)$ with a k^{-p} high-wavenumber spectrum where $p < 2$ must have singularities that are worse than isolated discontinuities. These singularities can be either isolated accumulating discontinuities or non-isolated discontinuities (see figure 1*b*). In either case the set of points of discontinuity can have a well-defined Kolmogorov capacity (or fractal dimension) D'_K in which case $p = 2 - D'_K$ (Vassilicos & Hunt 1991) and the anomalous decay (1.2) becomes

$$\frac{\overline{\theta^2}(0) - \overline{\theta^2}(t)}{\overline{\theta^2}(0)} \sim \left(\frac{2\kappa t}{L^2}\right)^{(1-D'_K)/2} + O\left(\frac{\kappa t}{L^2}\right), \tag{1.3}$$

valid both for spiral-like (isolated accumulation) and for fractal (non-isolated) sharp gradients or discontinuities. The anomalous decay also implies that the scalar dissipation rate $\chi = -(\mathrm{d}/\mathrm{d}t)\overline{\theta^2}(t) \sim \kappa^{(1-D'_K)/2} t^{-(1+D'_K)/2}$ at leading order. In the limit where $\kappa \to 0$ and if $D'_K \to 1$, i.e. if the spiral-like or fractal set of high gradients is space filling, the dissipation rate is then asymptotically independent of κ.

A relatively simple fluid mechanical situation where an isolated accumulating, in fact spiral, singularity is formed is when a two-dimensional vortex wraps a scalar field around itself. However, in spite of the relative simplicity of such a fluid mechanical configuration, its study goes beyond the sole molecular decay of singular geometry and takes into account the dynamic interplay of diffusion and evolving spiral accumulation because the accumulation is continuously created by advection. In this paper, we seek solutions of

$$\frac{\partial}{\partial t}\theta + \boldsymbol{u}\cdot\nabla\theta = \kappa\nabla^2\theta \tag{1.4}$$

with an appropriate velocity field $\boldsymbol{u}$ that can generate a spiral accumulation in the passive scalar field θ.

In §2 we consider a steady vortex with azimuthal velocity component $u_\phi(r) = r\Omega(r)$ and vanishing radial and axial velocity components. Hence the evolution of the two-dimensional advected and diffusing scalar field is governed by

$$\frac{\partial}{\partial t}\theta + \Omega(r)\frac{\partial}{\partial \phi}\theta = \kappa\nabla^2\theta \tag{1.5}$$

in the azimuthal plane (r, ϕ). We choose an angular velocity $\Omega(r) \sim r^{-s}$.

The decay of a scalar field in such a vortex is accelerated by two different effects. One is well known and is caused by the shear in the differential rotation which enhances scalar gradients *locally* and thereby accelerates their diffusion. This effect determines that the diffusive time scale T_D over which all scalar gradients have decayed scales with $\kappa^{-1/3}$ rather than κ^{-1} (Moffatt & Kamkar 1983; Rhines & Young 1983). However, the studies of Moffatt & Kamkar (1983) and Rhines & Young (1983) do not consider the effect of the scalar spiral geometry that is generated by the differential rotation of the vortex. This is a *global* effect which, as we show in §2, operates over time scales smaller than T_D and accelerates scalar dissipation in a way that is largely determined by the Kolmogorov capacity D'_K of the scalar spiral structure. The Kolmogorov capacity is a measure of the space-filling property of the spiral and is a function of the power s.

A vortical velocity field with an angular velocity $\Omega(r) \sim r^{-s}$ in a finite range of radii r can (at least in principle) be realized in the laboratory between two rotating porous circular walls where the fluid is injected in through the outer wall and sucked out through the inner wall. This flow is an analytical solution of the two-dimensional Navier–Stokes equations and in §3 we show that the analysis of §2 can be extended to this flow.

In §4 we confirm numerically the asymptotic analysis presented in the preceeding sections and we demonstrate the advantage of using D'_K as a measure of its space-filling property. Finally, we conclude in §5.

2. Passive scalar in a vortex

We now study the decay of a passive tracer θ in a steady vortex. The vortex is assumed to have an azimuthal component $u_\phi(r) = r\Omega(r) = R_0\Omega_0(r/R_0)^{1-s}$ and vanishing radial and axial velocity components. Note that this velocity field is an incompressible solution of the Euler equation for any value of s. We choose $s > 1$ to ensure that $u_\phi(r)$ decreases with increasing r.

The initial scalar field $\theta_0 = \theta(\boldsymbol{x}, t = 0)$ is on–off and defined by a regular interface between $\theta_0 = 1$ and $\theta_0 = 0$ with minimal distance r_0 and maximal distance R_0 from the rotation axis (see figure 2). By 'regular' we mean an interface without structure on scales much smaller than R_0. As time proceeds, the patch winds around the vortex, builds up spiral structure and decays because of molecular diffusion. The characteristic time Ω_0^{-1} is the inverse angular velocity of the vortex at R_0. This defines a Péclet number $Pe = \Omega_0 R_0^2 \kappa^{-1}$.

With the exception of §2.3.1 and (3.1)–(3.3), from now on we use the following non-dimensional notation throughout this paper:

$$R_0^{-1}r \to r, \quad \Omega_0 t \to t, \quad \Omega_0^{-1}\Omega(r) \to \Omega(r), \quad R_0^2\nabla^2 \to \nabla^2.$$

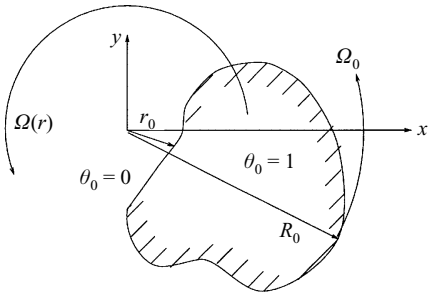

FIGURE 2. A scalar patch in the vicinity of a vortex which is placed at $\boldsymbol{x} = 0$.

In this notation (1.5) becomes

$$\frac{\partial}{\partial t}\theta + \Omega(r)\frac{\partial}{\partial \phi}\theta = \frac{1}{Pe}\nabla^2\theta \tag{2.1}$$

with $\Omega(r) = r^{-s}$, and r_0 represents r_0/R_0 whilst $R_0 = 1$.

The aim of the asymptotic analysis in this section is to characterize the decay of the scalar by calculating

$$\Delta E_\theta(t) = \overline{\theta^2}(0) - \overline{\theta^2}(t) \tag{2.2}$$

where the scalar variance $\overline{\theta^2}(t)$ is defined by

$$\overline{\theta^2}(t) = \int |\theta(r, \phi, t)|^2 r \mathrm{d}r\mathrm{d}\phi. \tag{2.3}$$

2.1. *Asymptotic analysis*

The analysis is based on the observation that if $\kappa = 0$, $\theta(r, \phi, t)$ is determined by the initial condition $\theta_0(r, \phi)$ and $\Omega(r)$ in a simple way. Indeed, the inviscid solution is given by a transformation of the initial conditions from Eulerian to Lagrangian coordinates. Generalizing this transformation to the diffusive case enables us to find an asymptotic solution of (2.1) which is then used to calculate $\Delta E_\theta(t)$.

In the case of vanishing diffusivity, (2.1) simplifies to

$$\frac{\partial}{\partial t}\theta + \Omega(r)\frac{\partial}{\partial \phi}\theta = 0, \tag{2.4}$$

and $\theta(r, \phi, t) = \Theta(r, \phi - \Omega(r)t, t)$ is a solution of (2.4) provided that $(\partial/\partial t)\Theta = 0$. Hence, $\theta(r, \phi, t) = \Theta(r, \phi - \Omega(r)t, 0) = \theta_0(r, \phi - \Omega(r)t)$ and the solution $\theta(r, \phi, t)$ is therefore given by

$$\theta(r, \phi, t) = \theta_0(r, \phi - \Omega(r)t). \tag{2.5}$$

Using the 2π-periodicity in ϕ, $\theta_0(r, \phi) = \sum_n f_n(r) \exp[\mathrm{i}n\phi]$ which implies that

$$\theta(r, \phi, t) = \sum_n f_n(r) \exp[\mathrm{i}n(\phi - \Omega(r)t)], \tag{2.6}$$

where the $f_n(r)$ are Fourier coefficients of the initial field θ_0. For an initial field defined by a regular interface as in figure 2, $f_n(r)$ varies as $1/n$ because of the isolated discontinuity at the boundary of the patch. For example, the initial condition in figure 6(*a*) is given exactly by

$$\left.\begin{aligned} f_n(r) &= \mathrm{i}/(2\pi n)\,(\exp(-\mathrm{i}n\pi) - 1)H(1 - r)H(r - r_0), \quad n \neq 0 \\ f_0(r) &= \tfrac{1}{2}\,H(1 - r)H(r - r_0) \end{aligned}\right\} \tag{2.7}$$

where H denotes the Heaviside function.

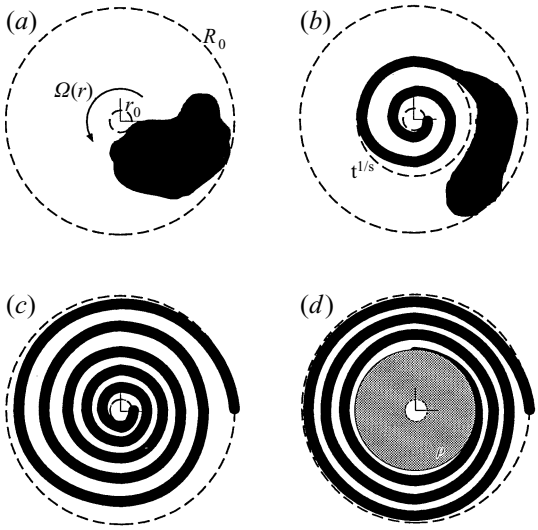

FIGURE 3. Schematic evolution of the scalar patch in the vicinity of a strong vortex, with $Pe \gg 1$. (*a*) The initial blob. (*b*) Spiral structure starts to build up and (*c*) expands throughout the patch. (*d*) The accumulation of gradients eventually leads to fast scalar decay which grows from the centre of the vortex with ρ in this figure being the radius over which the scalar has diffused.

In the case of finite diffusivity, we seek a solution of (2.1) in the form

$$\theta(r,\phi,t) = \sum_n f_n(r,t)\exp[\mathrm{i}n(\phi - \Omega(r)t)], \tag{2.8}$$

where the Fourier coefficients $f_n(r,t)$ are time-dependent and the initial condition is fully specified by $f_n(r,0)$. Introducing (2.8) into (2.1), we find that the evolution of $f_n(r,t)$ is governed by

$$\frac{\partial}{\partial t}f_n = \frac{1}{Pe}\left\{\frac{\partial^2}{\partial r^2}f_n + \left(-2\mathrm{i}nt\Omega' + \frac{1}{r}\right)\frac{\partial}{\partial r}f_n - \left(\underbrace{n^2\Omega'^2t^2}_{\text{(i)}} + \mathrm{i}n\Omega''t + \mathrm{i}n\frac{\Omega'}{r}t + \underbrace{\frac{n^2}{r^2}}_{\text{(ii)}}\right)f_n\right\} \tag{2.9}$$

where the prime denotes a derivative with respect to r.

Different time regimes in the evolution of the scalar patch can be readily identified. First, if $t < \Omega(r_0)^{-1} = r_0^s$, the vortex has not yet affected the patch and no spiral structure has developed (figure 3*a*). Secondly, if $r_0^s < t < \Omega(1)^{-1} = 1$, two distinct regions exist, the inner affected part of the patch, $r < t^{1/s}$, and the unaffected outer part, $r > t^{1/s}$ (figure 3*b*). Finally, if $t > 1$, the entire scalar field has developed spiral structure, provided, of course, that the Péclet number is large enough for the molecular diffusion not to have smoothed out that spiral structure (figure 3*c, d*). We mostly concentrate on times $t > 1$ because the main interest of this study is focused on anomalous decay during times when the patch becomes independent of the initial structure, that is, times when the entire patch is wrapped around the vortex. However, we will also briefly discuss earlier times, $r_0^s < t < 1$, at the end of this section.

The spiral near-singularity is taken into account by the transformation from ϕ to $\phi - \Omega(r)t$ in (2.8) and it is reasonable to assume that the coefficients f_n are regular

for all r and $t > 0$. Hence, if $t \gg 1$, and for all $r \leqslant 1$ and $|n| \geqslant 1$, the dominant contribution in the right-hand side of (2.9) comes from the term labelled (i), and (2.9) reduces to

$$\frac{\mathrm{d}f_n}{\mathrm{d}t} = -Pe^{-1}n^2\Omega'^2t^2f_n \tag{2.10}$$

at leading order. Note that we have made use of the assumption of regularity in $f_n(r,t)$ to obtain (2.10). The general solution to (2.10) is

$$f_n(r,t) = f_n(r,0)\exp\left[-\tfrac{1}{3}n^2\Omega'^2Pe^{-1}t^3\right]. \tag{2.11}$$

From(2.3),(2.8) and (2.11) it follows that the scalar variance $\overline{\theta^2}(t)$ can be computed from the amplitudes f_n as follows:

$$\begin{aligned}\overline{\theta^2}(t) &= \sum_n \int_{r_0}^1 |f_n(r,t)|^2\, r\,\mathrm{d}r \\ &= \sum_n \int_{r_0}^1 |f_n(r,0)|^2 \exp\left[-\tfrac{2}{3}n^2\Omega'^2Pe^{-1}t^3\right]\, r\,\mathrm{d}r.\end{aligned} \tag{2.12}$$

Because $f_n(r,0)$ is independent of r in the range $r_0 < r < 1$ we set $f_n = f_n(r,0)$. We define a critical radius ρ such that $\frac{2}{3}n^2\Omega'^2(\rho)Pe^{-1}t^3 = 1$, which implies

$$\rho = \left[\tfrac{2}{3}n^2s^2Pe^{-1}t^3\right]^{1/(2(s+1))}. \tag{2.13}$$

For $r \gg \rho$ we can use the approximation $\exp\left[\frac{2}{3}n^2\Omega'^2(r)Pe^{-1}t^3\right] \approx 1$, and if $r_0 < \rho \ll 1$ the integrals in (2.12) are therefore well approximated by

$$\begin{aligned}&\int_{r_0}^1 |f_n(r,0)|^2 \exp[-\tfrac{2}{3}n^2\Omega'^2Pe^{-1}t^3]\, r\,\mathrm{d}r \\ &\qquad\approx |f_n|^2 \int_{r_0}^{\rho} \exp[-\tfrac{2}{3}n^2\Omega'^2Pe^{-1}t^3]\, r\,\mathrm{d}r + |f_n|^2\tfrac{1}{2}(1-\rho^2).\end{aligned} \tag{2.14}$$

The critical radius ρ can be thought of as a diffusive length scale over which the harmonics in n have diffused. Therefore, the assumption that $\rho \ll 1$ means that spiral structure exists in the range $\rho < r < 1$, as for example shown in figure 3(d). The condition $r_0 < \rho \ll 1$ requires (omitting constants of order unity) that

$$r_0^{2(s+1)/3}\left[(ns)^{-2}Pe\right]^{1/3} < t \ll \left[(ns)^{-2}Pe\right].^{1/3} \tag{2.15}$$

It is sufficient that $r_0^{2(s+1)/3}(s^{-2}Pe)^{1/3} < t$ for r_0 to be smaller than ρ for all values of n and it is necessary that $t \ll (s^{-2}Pe)^{1/3}$ for ρ to be much smaller than 1 for at least some values of n. Such values of n are bounded, $|n| < N$ where N is determined by $\rho(N) = 1$ and therefore $N = s^{-1}[Pe\ t^{-3}]^{1/2}$. It follows that the present analysis is valid in the range of times

$$\max\left[1, r_0^{2(s+1)/3}\left(s^{-2}Pe\right)^{1/3}\right] \ll t \ll \left(s^{-2}Pe\right)^{1/3}, \tag{2.16}$$

a range that can only exist if $Pe \gg s^2$; s is a parameter of the local shear of the vortex and is usually of order 1, for example $s = 2$ for a point vortex. That is, we consider very large Péclet numbers, $Pe \gg 1$. In the time range (2.16) the decay of the

scalar variance is well approximated by

$$\overline{\theta^2}(0)-\overline{\theta^2}(t)\simeq\frac{1}{2}\sum_{|n|<N}|f_n|^2\left(\rho^2-\int_{r_0}^{\rho}\exp\left[-\tfrac{2}{3}n^2\Omega'^2Pe^{-1}t^3\right]\,r\,\mathrm{d}r\right)$$
$$+\frac{1}{2}\sum_{|n|>N}|f_n|^2\left(1-\int_{r_0}^{1}\exp\left[-\tfrac{2}{3}n^2\Omega'^2Pe^{-1}t^3\right]\,r\,\mathrm{d}r\right). \qquad (2.17)$$

As mentioned before, any initial on–off scalar patch defined by a regular interface is of the form $f_n\sim n^{-1}$. Thus, the series in (2.17) are of the form $\sum n^{-2s/(s+1)}$ and $\sum n^{-2}$. They converge for all $s>1$, a condition which was imposed earlier to ensure an accumulating scalar pattern at the centre.

Truncating all the terms with $|n|>N$ in the series (2.17) because these terms decay exponentially, noting that $\rho^2\gg\int_{r_0}^{\rho}\exp\left[-\frac{2}{3}n^2\Omega'^2Pe^{-1}t^3\right]\,r\,\mathrm{d}r$ for $|n|<N$ and omitting constants of order unity (in particular the series in n), we obtain the main scaling result of this section

$$\overline{\theta^2}(0)-\overline{\theta^2}(t)\sim\left(Pe^{-1/3}t\right)^{3/(s+1)}, \qquad (2.18)$$

valid in the time range (2.16). The spiral structure of the scalar field is conveniently characterized by a Kolmogorov capacity D'_K, which as we show numerically in §4 is independent of time in the spiral time range where it is related to the vortex scaling exponent s by $D'_K=s/(s+1)$ (see §4). The Kolmogorov capacity is a measure of the spiral's accumulation rate; D'_K is close to 1 if this accumulation rate is very slow and the spiral is close to space-filling and D'_K is significantly smaller than 1 for faster accumulation rates and less-space-filling spirals. Here $1/2<D'_K<1$ because $s>1$, and the result (2.18) can be recast in the form

$$\overline{\theta^2}(0)-\overline{\theta^2}(t)\sim\left(Pe^{-1/3}t\right)^{3(1-D'_K)}. \qquad (2.19)$$

The advantage of casting this result in terms of D'_K rather than s is that D'_K has a direct visual interpretation in terms of the spiral structure of the scalar field, whereas s is related to the underlying velocity field. In particular, D'_K can be more easily and directly measured than s and we also find in §4 that D'_K can be measured accurately even when the resolution is not sufficient to reveal the decay law (2.19).

2.2. *The spiral time range*

The result (2.18)–(2.19) is valid in the time range (2.16) which exists in the limit $Pe\gg1$. We call this time range the 'spiral time range' and write it as follows:

$$T_S\ll t\ll T_D \qquad (2.20)$$

where

$$T_S=\max[1,r_0^{2/(3-3D'_K)}Pe^{1/3}],\quad T_D=Pe^{1/3}. \qquad (2.21)$$

omitting the prefactors $s^{-2/3}$ because s is usually of order 1, and assuming that $D'_K=s/(s+1)$ independently of time throughout the spiral time range. The numerical results of §4 support this assumption.

The upper time limit T_D is the diffusive time scale of the patch. The scaling $T_D\sim Pe^{1/3}$ (rather than $T_D\sim Pe$ as in the case of molecular diffusion without a shear-generating velocity field) has been derived in earlier studies (Moffatt & Kamkar 1983; Rhines & Young 1983). This scaling $T_D\sim Pe^{1/3}$ reflects the accelerating effect of the differential rotation's local shear and is independent of the spiral's accumulation

rate, i.e. of D'_K. For time scales much smaller than T_D, the accumulating structure of scalar gradients has its own accelerating effect on scalar diffusion, and it is reflected in the scaling law (2.19). Thus, we may summarize the main result of this section as follows: the presence of *local* shear in the vortex determines the diffusive time scaling $T_D \sim Pe^{1/3}$; the presence of a spiral accumulation of scalar gradients is a *global* effect that manifests itself in the anomalous decay (2.19) in the spiral time range.

The lower time limit T_S of this time range is always larger than 1 which ensures that the vortex has had the time to fully wrap the scalar patch around itself. $T_S \sim 1$ when $r_0 \ll Pe^{(D'_K-1)/2}$, but when $Pe^{(D'_K-1)/2} \ll r_0 < 1$ then $T_S \sim r_0^{2/(3-3D'_K)} Pe^{1/3}$ and the spiral time range is preceeded by a different range, $1 \ll t \ll T_S$, where the scalar variance decays differently. Whereas (2.19) remains valid in the spiral range, in the range $1 \ll t \ll T_S$ the approximation (2.14) must be replaced by

$$\int_{r_0}^{1} |f_n(r,0)|^2 \exp[-\tfrac{2}{3}n^2\Omega'^2 Pe^{-1}t^3]\, r\, \mathrm{d}r \approx |f_n|^2 \tfrac{1}{2}(1-r_0^2), \tag{2.22}$$

because in this range $\rho < r_0$, and a similar analysis leads to

$$\overline{\theta^2}(0) - \overline{\theta^2}(t) \simeq \left(Pe^{-1/3}t\right)^{3/2}. \tag{2.23}$$

This behaviour can be observed before the spiral accumulation's global effect. If these early times $1 \ll t \ll T_S$ exist the patch is too narrow to form a well-defined accumulating spiral pattern, and the diffusion is accelerated by the local shear of the vortex only.

Finally, we comment on the limit $t \gg 1$ which has been imposed so far. Because $r_0^{2/(3-3D'_K)} Pe^{1/3} \to 0$ as $r_0 \to 0$, we might expect anomalous behaviour for times where only part of the patch is sheared out into spiral structure, that is times $r_0^s < t < 1$. Indeed, it is shown in the Appendix that the decay of the inner part of the patch, $r_0 < r < t^{1/s}$, is again dominated by term (i) in (2.9). The decay of the outer part, $t^{1/s} < r < 1$, which is not sheared by the vortex, is dominated by term (ii). The overall decay can be written as follows:

$$\overline{\theta^2}(0) - \overline{\theta^2}(t) \simeq \left(Pe^{-1/3}t\right)^{3(1-D'_K)} + \left(Pe^{-1}t\right)^{1/2} \tag{2.24}$$

where the first term of the right-hand side is the contribution of the inner part $r < t^{1/s}$ whilst the second term is the contribution of the outer part $r > t^{1/s}$. Note that the term $(Pe^{-1}t)^{1/2}$ can be neglected even for times $t < 1$ if $1/2 < D'_K < 5/6$.

2.3. *The accelerating effect of the spiral on the scalar decay rate*

In the spiral time range the enhancement of diffusion and scalar dissipation is due to the presence of a spiral near-singularity in the scalar field. This effect of the spiral near-singularity is the same as the effect that a fractal field has on its dissipation. It is a *global* effect originating in the *space-filling* properties of spirals and fractals and must be distinguished from the effect that shear can have on dissipation which is a local effect because shear is a local gradient.

2.3.1. *Anomalous diffusion of fractal or spiral structures*

In the simpler case of an initially spiral or fractal on–off field evolving under the action of molecular diffusion alone (the case of (1.1)–(1.3)), Vassilicos (1995) brings out the effect of the space-filling property on the dissipation by considering the diffusive length scale $\delta(t) \equiv \mathscr{L}(t) - \mathscr{L}(0)$ where $\mathscr{L}(t)$ is the correlation length scale.

Unlike the rest of §2, the notation for lengths, times and wavenumbers is dimensional in this subsection. The diffusive length scale $\delta(t)$ is a measure of the distance over which the effects of molecular diffusion are appreciable on the structure at time t. For one-dimensional fields $\theta(x,t)$

$$\mathscr{L}(t) = \int_0^\infty k^{-1} \frac{\Gamma(k,t)}{\overline{\theta^2}(t)} \mathrm{d}k \tag{2.25}$$

where $\Gamma(k,t)$ is the time-dependent Fourier power spectrum of $\theta(x,t)$. For fields $\theta(\mathbf{x},t)$ of higher dimensionality, e.g. two-dimensional fields as in most of this paper, (2.25) remains exact under the assumption of isotropy for $\theta(\mathbf{x},t)$. The diffusive length scale of one-dimensional fields evolving according to (1.1) can be estimated for short times $\kappa t/L^2 \ll 1$,

$$\delta(t) \sim (\kappa t)^{1/2} \left((\kappa t)^{1/2}\right)^{-D'_K}, \tag{2.26}$$

where D'_K is the Kolmogorov capacity of the points of discontinuity of the initial on–off scalar field $\theta(x,0)$. $\Gamma(k,t) \sim k^{-2+D'_K}$ is used to obtain (2.26), see Vassilicos (1995).

The Kolmogorov capacity D'_K is defined by the number of boxes N of length l needed to cover all the points of the set if $N(l) \sim l^{-D'_K}$. This definition implies

$$\delta(t) \sim (\kappa t)^{1/2} \, N\left((\kappa t)^{1/2}\right) \tag{2.27}$$

for the early times of decay which means that the diffusive length scale $\delta(t)$ is proportional to the total length of the fractal covering by segments of size $(\kappa t)^{1/2}$. The closer D'_K is to 1, the more space filling the covering by segments of size $(\kappa t)^{1/2}$, the larger the diffusive length scale $\delta(t)$, and therefore the faster the early decay by diffusive attrition.

Similar arguments can be reproduced for the artificial situation where a two-dimensional spiral initially on–off scalar field decays according to (1.1). In this case the Fourier power spectrum is given by $\Gamma(k,t) \sim k^{-3+2D'_K}$ and thus

$$\delta(t) \sim \left[(\kappa t)^{1/2} \left((\kappa t)^{1/2}\right)^{-D'_K}\right]^2 \tag{2.28}$$

where D'_K is now the Kolmogorov capacity of the intersection of the spiral with a straight line. By definition of the Kolmogorov capacity,

$$\delta(t) \sim \left[(\kappa t)^{1/2} \, N\left((\kappa t)^{1/2}\right)\right]^2, \tag{2.29}$$

and comparison with (2.27) suggests that the power 2 on the right-hand side of (2.29) is nothing but the Euclidean dimensionality of the embedding space. Again, the global effect originates in the space-filling property of the spiral and is manifest in (2.29). The diffusive length scale is larger for larger values of D'_K, i.e. for more-space-filling spirals, which reflects a faster dissipation rate.

It should be noted that the diffusive length scale $\delta(t)$ is not the inner cutoff length scale $\eta(t)$ of the fractal or spiral field's power spectrum. The global effect of the spiral or fractal structure of gradients originates in the slope of the self-similar Fourier power spectrum of such structures. In the case of one-dimensional on–off fields the power spectrum scales as $k^{-2+D'_K}$ in the range $L^{-1} \ll k \ll \eta(t)^{-1}$. Hence we can estimate the effect of the spiral or fractal space-filling property on the variance $\overline{\theta^2}(t)$ as follows:

$$\overline{\theta^2}(t) \sim \int_{L^{-1}}^{\eta(t)^{-1}} k^{-2+D'_K} \mathrm{d}k. \tag{2.30}$$

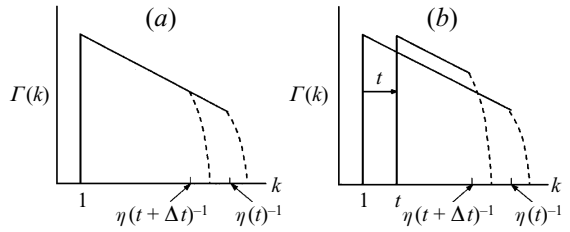

FIGURE 4. (*a*) Spectral picture of a diffusing fractal or spiral structure; the dashed line indicates the exponential decay at high wavenumbers where diffusion acts. (*b*) In the case of a continuously acting vortex, diffusion not only removes high wavenumbers, but the entire spectrum is shifted towards higher wavenumbers as time advances.

At $t = 0$, $\eta = 0$, and therefore

$$\overline{\theta^2}(0) - \overline{\theta^2}(t) \sim \int_{\eta(t)^{-1}}^{\infty} k^{-2+D'_K}\,\mathrm{d}k \tag{2.31}$$

which leads to the right conclusion $\overline{\theta^2}(0) - \overline{\theta^2}(t) \sim (\kappa t)^{(1-D'_K)/2}$ in the limit where $\eta(t) \ll L$ only if $\eta(t) \sim (\kappa t)^{1/2}$. Hence the diffusive length scale $\delta(t)$ is larger than the inner cutoff length scale $\eta(t)$, and in fact (2.27) can be recast as

$$\delta(t) \sim \eta(t)\, N[\eta(t)]. \tag{2.32}$$

2.3.2. *Passive scalar in a vortex*

To bring out the effect of the space-filling property on dissipation when the vortex continously creates spiral structure as time advances, we need to consider an appropriately defined diffusive length scale $\delta(t)$. To calculate the integral length scale $\mathscr{L}(t)$ using (2.25) we need to know the time-dependent scalar power spectrum $\Gamma(k,t)$. Gilbert (1988) discusses the self-similar power spectra of a patch wrapping around a vortex in detail. He identifies the spiral range of length scales in which $\Gamma(k) \sim k^{-3+2D'_K}$ as before. However, the essential difference with an initially spiral field that decays under the sole action of molecular diffusion is that the vortex continuously creates spiral structure as time advances. Hence, the spiral range of length scales is continuously shifted towards smaller scales (i.e. higher wavenumbers), see figure 4, and $\Gamma(k,t) \sim t^{2(1-D'_K)}k^{-3+2D'_K}$ in the range of scales $k > t$ with $t > 1$. Non-dimensional wavenumbers are defined by $R_0 k \to k$.

The correlation length scale $\mathscr{L}(t)$ defined by (2.25) becomes

$$\begin{aligned}\mathscr{L}(t) &\sim \int_t^{\infty} k^{-1} \frac{t^{2(1-D'_K)}k^{-3+2D'_K}}{1 - \left(Pe^{-1/3}t\right)^{3(1-D'_K)}}\,\mathrm{d}k \\ &\sim t^{-1}\left[1 + \left(Pe^{-1/3}t\right)^{3(1-D'_K)}\right]\end{aligned} \tag{2.33}$$

for short times $t < Pe^{1/3}$. $\mathscr{L}(t)$ is now determined by two competing effects: the continued action of the vortex decorrelates the scalar field by enhancing gradients, $\mathscr{L}(t) \sim t^{-1}$, whereas diffusion smooths out gradients and thus correlates the scalar field, $\mathscr{L}(t) \sim 1 + (Pe^{-1/3}t)^{3(1-D'_K)}$. To isolate the diffusive effect we redefine the diffusive length scale

$$\delta(t) \equiv \frac{\mathscr{L}(t)}{\mathscr{L}^{\mathrm{i}}(t)} - \frac{\mathscr{L}(1)}{\mathscr{L}^{\mathrm{i}}(1)} \tag{2.34}$$

where $\mathscr{L}^i$ is the inviscid correlation length scale with $\mathscr{L}^i \sim t^{-1}$ because $\overline{\theta^2}(t) = \text{const}$ if $\kappa = 0$. Thus the diffusive length scale increases as

$$\delta(t) \sim \left(Pe^{-1/3}t\right)^{3(1-D'_K)} \tag{2.35}$$

which can be recast as

$$\delta(t) \sim \left[(Pe^{-1}t^3)^{1/2}\, N\left((Pe^{-1}t^3)^{1/2}\right)\right]^2 \tag{2.36}$$

analogously to (2.29). The diffusive length scale is proportional to the square of the total length of the spiral covering by N segments of size $(Pe^{-1}t^3)^{1/2}$; $(Pe^{-1}t^3)^{1/2}$ is the length scale characterizing diffusion locally for single sharp scalar gradients in a shear-dominated flow and has been derived before in the studies of Moffatt & Kamkar (1983) and Rhines & Young (1983). This length scale in real space has to be contrasted with the inner cutoff scale $\eta(t)^{-1}$ of the spiral field's power spectrum in wavenumber space. If we approximate the decay of the scalar field using the field's power spectrum analogously to (2.31) by

$$\overline{\theta^2}(1) - \overline{\theta^2}(t) \sim \int_{\eta(t)^{-1}}^{\infty} t^{2-2D'_K} k^{-3+2D'_K}\, \mathrm{d}k, \tag{2.37}$$

we recover the right conclusion (2.19) only if $\eta(t) \sim (Pe^{-1}t)^{1/2}$.

The local acceleration of diffusion by the shear is reflected in $(Pe^{-1}t^3)^{1/2} > (Pe^{-1}t)^{1/2}$. On the other hand, the global acceleration of diffusion is reflected in the diffusive length-scale $\delta(t)$ which is a measure of the spatial extent over which diffusion has erased the spiral structure. It is the space-filling property of the spiral gradients that leads to $\delta(t) > (Pe^{-1}t^3)^{1/2}$ and therefore to the accelerated diffusion (2.19) which determines the decay of the entire patch.

Figure 6 in §4 clarifies the accelerating effect of the spiral's space-filling property on diffusion. Whereas the gradients of the outer arms (which diffuse over the shear-dominated scale $(Pe^{-1}t^3)^{1/2}$) are still sharply defined in figure 6(*c*), the inner gradients (where the accumulation of gradients determines the diffusive length scale) are already smoothed out. We find numerically in §4 that the spatial extent of this smoothed-out core has the same time-dependence as the critical radius ρ, and using (2.13) with $D'_K = s/(s+1)$ it turns out that

$$\delta(t) \sim \rho^2(t). \tag{2.38}$$

3. Passive scalar between two porous rotating cylinders

In the previous section we assumed $\Omega(r) \sim r^{-s}$. This model flow could form the basis of an oversimplified picture of the flow in the vicinity of strong vortices in two-dimensional turbulence, and the locally two-dimensional flows around vortex tubes in three-dimensional turbulence. Trailing vortices behind airfoils have also been proposed to have such power-law behaviour (Saffman 1992).

However, exact solutions of the two-dimensional Navier–Stokes equations with $\Omega(r) \sim r^{-s}$ for various values of s are known for the flow between two rotating porous cylinders (see, for example, Lugt 1983). Fluid is injected in through the outer wall and sucked out through the inner wall; the suction velocity V is defined at the inner radius R_1. The radii and rotation rates of the cylinders are R_1, R_2 and Ω_1, Ω_2, respectively. Refer to figure 5 for a sketch of the flow. The axial and radial velocity

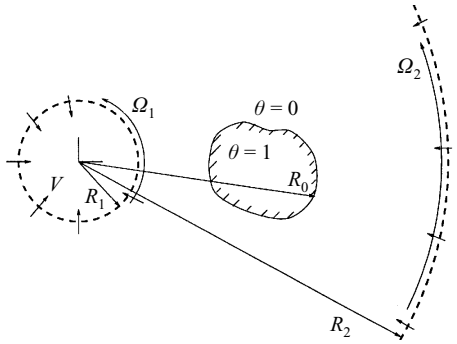

FIGURE 5. A scalar patch in the flow field of two rotating, porous cylinders.

components are (in dimensional units)

$$u_r = -\frac{VR_1}{r}, \quad u_\phi = r\Omega(r), \tag{3.1}$$

where the angular velocity $\Omega(r)$ is found from the u_ϕ momentum equation and can be written as

$$\Omega(r) = \Omega_1 \left[\frac{\sigma^{Re} - \lambda}{\sigma^{Re} - \sigma^2} \left(\frac{r}{R_1} \right)^{-2} + \frac{\lambda - \sigma^2}{\sigma^{Re} - \sigma^2} \left(\frac{r}{R_1} \right)^{-Re} \right] \tag{3.2}$$

for $Re \neq 2$†, where the Reynolds number Re and the parameters σ and λ are given by

$$\sigma = \frac{R_1}{R_2}, \quad \lambda = \frac{\Omega_2}{\Omega_1}, \quad Re = \frac{R_1 V}{\nu}, \tag{3.3}$$

where ν is the kinematic viscosity of the fluid. Interestingly, for a suitable choice of σ, λ we recover $\Omega(r) \sim r^{-s}$ with $s = Re$. We note that (3.2) is valid throughout the flow, and in particular at the cylinder walls.

The evolution of a passive scalar in such a velocity field is governed by (1.4) as before.

For consistent notation with §2 (with scaling parameters Ω_0, R_0) we non-dimensionalize the angular velocity (3.2) and obtain

$$\Omega(r) = \beta \left[\frac{\sigma^{Re} - \lambda}{\sigma^{Re} - \sigma^2} \left(\frac{r}{\alpha} \right)^{-2} + \frac{\lambda - \sigma^2}{\sigma^{Re} - \sigma^2} \left(\frac{r}{\alpha} \right)^{-Re} \right], \tag{3.4}$$

with

$$\alpha = \frac{R_1}{R_0}, \quad \beta = \frac{\Omega_1}{\Omega_0}. \tag{3.5}$$

In what follows, we assume a suitable choice of parameters such that $\Omega(r) \sim r^{-Re}$.

The evolution equation of a scalar field (1.4) can now be written as

$$\frac{\partial}{\partial t}\theta - \frac{m}{r}\frac{\partial}{\partial r}\theta + \Omega(r)\frac{\partial}{\partial \phi}\theta = \frac{1}{Pe}\nabla^2\theta \tag{3.6}$$

with

$$m = \frac{Re\, Pr}{\alpha Pe}, \quad Pr = \frac{\nu}{\kappa}. \tag{3.7}$$

† $\Omega(r) = \Omega_1 \left[\dfrac{1}{(r/R_1)^2} + \dfrac{1 - \lambda/\sigma^2}{\ln \sigma} \dfrac{\ln(r/R_1)}{(r/R_1)^2} \right]$ for $Re = 2$.

As previously, the scalar is thought of as an initially smooth patch placed between the two cylindrical boundaries at minimal and maximal distances r_0 and 1 (see figure 5). It develops spiral structure because of the differential rotation between the cylinders and is slowly advected towards the centre because of the suction velocity. We consider here only times where the scalar has not reached the inner cylinder, $t < (r_0^2 - \alpha^2)/(2m)$. In the rest of this section we revise the analysis of §2.1.

We seek a solution along the coordinates of ideal particles

$$\theta(r, \phi, t) = \Theta(\xi, \eta, t) \tag{3.8}$$

with the Lagrangian coordinates

$$\xi = (r^2 + 2mt)^{1/2}, \quad \eta = \phi - \Omega(r)t. \tag{3.9}$$

Using the 2π-periodicity in ϕ, we therefore write

$$\theta(r, \phi, t) = \sum_n f_n(\xi, t) \exp[\mathrm{i}n\eta]. \tag{3.10}$$

Using (3.10) in (3.6), the evolution of the $f_n(\xi, t)$ is governed by

$$\frac{\partial}{\partial t} f_n = \frac{1}{Pe} \left\{ \frac{\partial^2}{\partial \xi^2} f_n + \frac{1}{\xi} \left(2 - \frac{r^2}{\xi^2}\right) \frac{\partial}{\partial \xi} f_n \right. \\ \left. + \left(\underbrace{-n^2 \Omega'^2 t^2}_{\text{(i)}} - \mathrm{i}n\Omega'' t - \mathrm{i}n\Omega' \frac{1}{r} t - \underbrace{\mathrm{i}n\Omega' \frac{Re\ Pr}{\alpha r} t}_{\text{(ii)}} - \frac{n^2}{r^2} \right) f_n \right\} \tag{3.11}$$

where the prime denote derivatives with respect to r. Similarly to the problem of §2, it is reasonable to assume that the coefficients $f_n(\xi, t)$ are regular in ξ for all r and $t > 0$. For large enough times, $t \gg 1$, where spiral structure has formed throughout the patch, and for all $r \leqslant 1$ and $|n| \geqslant 1$, the dominant contribution on the right-hand side of (3.11) comes from the term labelled (i) which implies the solution

$$f_n(\xi, t) = f_n(\xi, 0) \exp\left[-\tfrac{1}{3} n^2 \Omega'^2 Pe^{-1} t^3\right]. \tag{3.12}$$

The decay of the amplitudes is now given in Lagrangian coordinates but note also that $f_n(\xi, 0) = f_n(r, 0)$ initially. The effect of contracting differential rotation is incorporated in the term labelled (ii). It essentially leads to faster oscillations in the f_n and can be neglected for the decay at large times.

The scalar variance is computed from the amplitudes $f_n(\xi, t)$ as follows:

$$\overline{\theta^2}(t) = \sum_n \int_{\tilde{r}_0}^{\tilde{R}_0} |f_n(\xi, t)|^2 \, r \, \mathrm{d}r \\ = \sum_n \int_{\tilde{r}_0}^{\tilde{R}_0} |f_n(r, 0)|^2 \exp\left[-\tfrac{2}{3} Pe^{-1} n^2 \Omega'^2 t^3\right] r \, \mathrm{d}r \tag{3.13}$$

with integration boundaries $\tilde{r}_0 = (r_0^2 - 2mt)^{1/2}$ and $\tilde{R}_0 = (1 - 2mt)^{1/2}$. Assuming the f_n to be independent of r, $f_n(r, 0) = f_n$, and recalling the definition (2.13) of a critical

radius ρ, the integral in (3.13) can be approximated by

$$\int_{\tilde{r}_0}^{\tilde{R}_0} |f_n(r,0)|^2 \exp[-\tfrac{2}{3}n^2\Omega'^2 Pe^{-1}t^3]\, r\,\mathrm{d}r \approx |f_n|^2 \int_{\tilde{r}_0}^{\rho} \exp[-\tfrac{2}{3}n^2\Omega'^2 Pe^{-1}t^3]\, r\,\mathrm{d}r + |f_n|^2 \tfrac{1}{2}(1-2mt-\rho^2). \quad (3.14)$$

Recall that the definition of ρ leads to the time range

$$\max\left[1, r_0^{2(Re+1)/3}\left(Re^{-2}Pe\right)^{1/3}\right] \ll t \ll \left(Re^{-2}Pe\right)^{1/3}, \quad (3.15)$$

during which the approximation (3.14) is valid. Omitting constants of order unity, the decay of the scalar variance is obtained:

$$\overline{\theta^2}(0) - \overline{\theta^2}(t) \sim mt + (Pe^{-1/3}\,t)^{3(1-D'_K)}, \quad (3.16)$$

where

$$D'_K = \frac{Re}{Re+1}. \quad (3.17)$$

The first term on the right-hand side of (3.16) stems from the inwards flow and it leads to a further acceleration of the variance decay. The second term scales as before and if $mt \ll (Pe^{-1/3}\,t)^{3(1-D'_K)}$ we recover (2.19).

Summarizing, the anomalous decay

$$\overline{\theta^2}(0) - \overline{\theta^2}(t) \sim (Pe^{-1/3}\,t)^{3(1-D'_K)}, \quad (3.18)$$

is observable during the times

$$T_S \ll t \ll \min\left[\frac{r_0^2-\alpha^2}{2m}, \left(m^{-1}Pe^{-1+D'_K}\right)^{1/(3D'_K-2)}, T_D\right] \quad (3.19)$$

for this flow. T_S and T_D are defined as in (2.21), and the two other terms in the upper time limit are given by the conditions that no scalar leaves the inner cylindrical boundary and that the first term on the right-hand side of (3.16) is negligible. It is important to note that D'_K and the flow exponent s can be varied at will by varying the Reynolds number Re.

4. Numerical study

4.1. *Diffusion of the scalar patch*

To illustrate the asymptotic results from the previous sections we now study the evolution of a diffusing scalar in a vortex numerically. Equation (1.4) is solved on a cylindrical coordinate frame using a conservative finite-volume formulation. The discretization of the advective terms is based on a second-order limited high-resolution scheme combined with an explicit one-step time integration (Nikiforakis & Toro 1997).

The diffusive fluxes are treated as source terms, and to maintain second-order accuracy in time a fractional step method is employed (Strang 1968). Periodic boundary conditions are used in the azimuthal direction and homogeneous Neumann conditions in the radial direction.

Our interest focuses on the diffusive properties of the advected scalar in the presence of accumulating strong scalar gradients. The numerical dissipation introduced locally near the gradients is essential on the one hand to damp numerical oscillations, but it

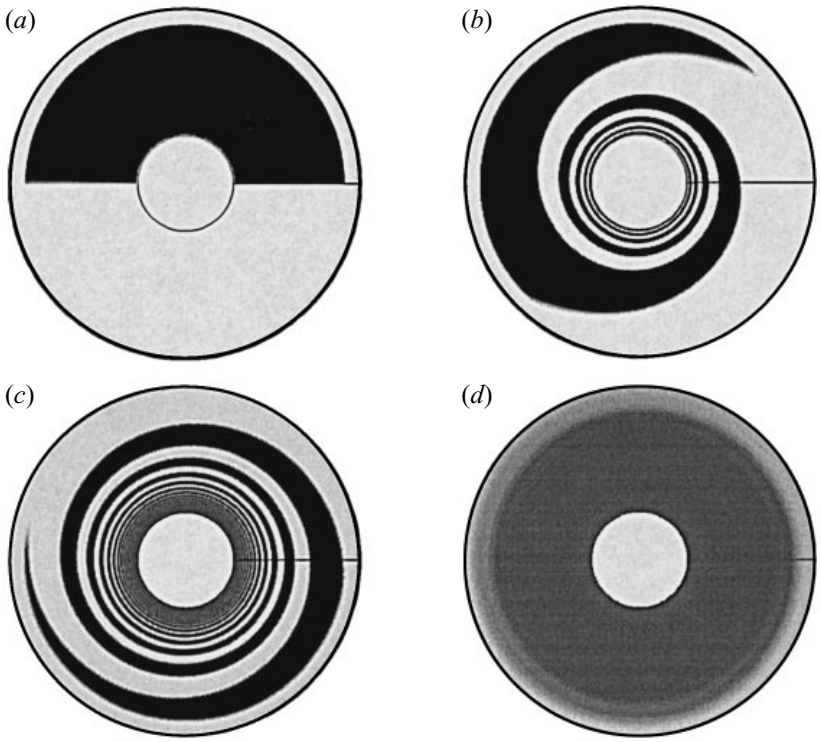

FIGURE 6. Evolution of a scalar spiral structure in a vortex of scaling exponent $s = 4$. Different periods of time are depicted. (*a*) The initial field. (*b*) Spiral structure starts to build up. (*c*) Spiral structure extends throughout the field and accelerated diffusion is observed at the core. Notice that the outer gradients are still sharply defined. The area of the inner diffused grey core grows rapidly with time in proportion to $\delta(t)$ – see (2.38), (2.35) and (2.36). The local diffusive length scale, i.e. the width of the scalar gradients, is given by $(Pe^{-1}t^3)^{1/2}$. (*d*) The entire patch is diffused.

may on the other hand affect the overall physical diffusive behaviour, in particular for the very high Péclet numbers that our asymptotic solutions require. Only numerical validation experiments can address this concern, and a detailed comparison of the numerically and analytically obtained transport of a single one-dimensional initial discontinuity allowed an estimation of the resolution requirements for the accurate prediction of the scalar variance decay over a given period of time by imposing an empirically determined maximum cell Péclet number.

We present here the results for simulations with varying vortex scaling exponent s, and initial conditions such as shown in figure 6(*a*), but with varying r_0. The Péclet number has been chosen to be $Pe = 10^5$. For an initial patch with $r_0 = 0.3$ the necessary grid resolution was then 800×800 grid points in the radial and azimuthal directions to sufficiently resolve the discontinuities. In the radial direction a smooth hyperbolic stretching was employed to increase the resolution near the centre of the vortex. The computational domain has a toroidal shape with the radial boundaries quite close to the patch. However, diffusion in the radial direction towards the boundaries was found to be very small during the times investigated here, and any additional 'diffusion' due to scalar leaving the computational domain is negligible.

Figure 6 shows a typical example of the evolution of a scalar patch by depicting instantaneous flow patterns at different times. The initial patch has been chosen to

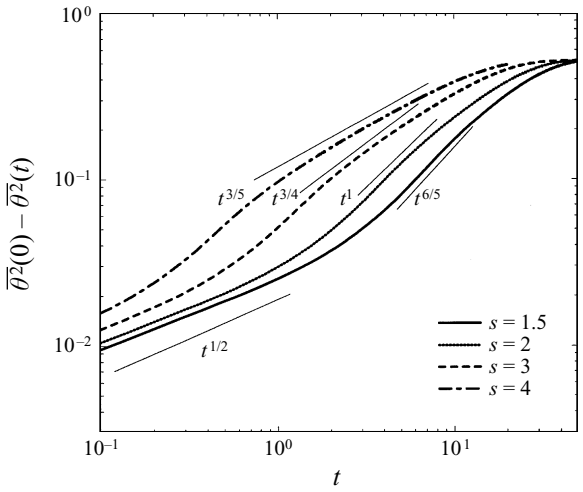

FIGURE 7. Numerical study of the diffusion of the scalar patch for different accumulation rates s. For early times ($t \ll 1$) normal diffusive behaviour is observed with $\overline{\theta^2}(0) - \overline{\theta^2}(t) \sim t^{1/2}$. In the spiral time range accelerated diffusion $\overline{\theta^2}(0) - \overline{\theta^2}(t) \sim t^{3(1-D'_K)}$ is observed. The expected asymptotic scaling behaviour is indicated by straight lines.

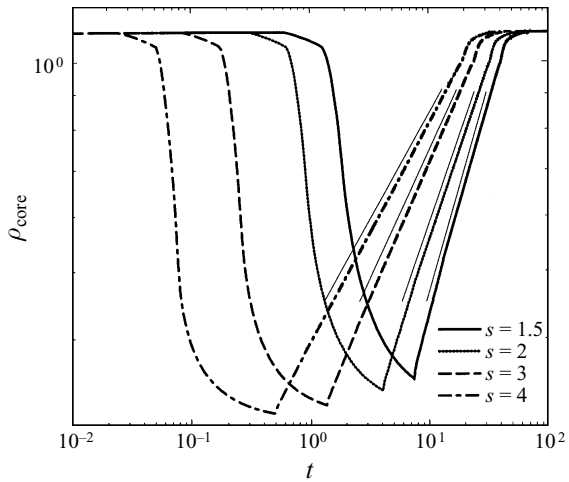

FIGURE 8. Variation of the radius of the smoothed-out core ρ_{core} in time for different accumulation rates s. The algorithm detects initially no structure in the scalar patch and ρ_{core} is only bounded by the computational domain, i.e. $\rho_{core} \leqslant 1.1$. Spiral structure builds up and ρ_{core} decreases until it reaches its minimum which is approximately $\rho_{core} \approx r_0 = 0.3$. As time advances further, this spiral structure is destroyed by diffusion and the smoothed-out core rises sharply according to $\rho_{core} \sim t^{3/(2(s+1))}$. The expected asymptotic scaling behaviour in this spiral time range is indicated with straight lines. For very large times when $\rho_{core} > R_0 = 1$ there is a slight change in the scaling (acceleration of diffusion during a short period of time) which is due to edge effects at the numerical boundaries.

fill the upper half-plane with limiting radii $[r_0, 1]$ which corresponds to the initial conditions given exactly by (2.7).

Figure 7 shows results for different accumulation rates s. Given the numerical restrictions in simulating the high Péclet number limit required by the asymptotic analysis, the accelerated diffusion given by (2.19) is quite clearly seen during the

1. Flow and geometry

$Pe = 10^5$ $Re = 4$ $Pr = 1$ $\lambda = 0$ $\beta = 144$ $m = 1.4 \times 10^{-4}$
$R_1 = 0.29$ $R_2 = 1.43$ $r_0 = 0.36$ $R_0 = 1$ $\alpha = 0.29$ $\sigma = 0.2$

2. Time limits

$$T_S = \max[1, r_0^{2(Re+1)/3}(Re^{-2}Pe)^{1/3}] = \max[1, 0.6] = 1$$

$$T_D = \min\left[\frac{r_0^2 - \alpha^2}{2m}, \left(m^{-1}Pe^{-1+D'_K}\right)^{1/(3D'_K-2)}, (Re^{-2}Pe)^{1/3}\right] = \min[160, 1.4 \times 10^7, 20] = 20$$

TABLE 1. Example of a flow configuration

spiral time range, $T_S \ll t \ll T_D$. For example, for $s = 4$ we predict $T_S = O(1)$ and $T_D = O(10)$ in agreement with the numerical result in figure 7. The straight lines are the asymptotic predictions for comparison with the numerical findings. Generally, there is a slight tendency to underestimate the decay rate particularly for very early times where theoretically $\overline{\theta^2}(0) - \overline{\theta^2}(t) \sim t^{1/2}$. Also, the numerical resolution does not allow great asymptotic scale separation, particularly for small values of s, and as a result, for small values of s the asymptotic decay is only a 'tangent' to the numerically observed anomalous decay.

A much better numerical measure of this anomalous decay and the spiral time range is the radius of the smoothed-out core. This radius we measure with an algorithm that counts the number of gradients in the radial direction, starting from the centre, and then averages in the azimuthal direction after having selected one particular gradient. In figure 8 we plot the result for the third gradient found in this way. The initial value of the radius detected by this algorithm reflects the size of the computational domain. Spiral structure builds up and the radius measured by this algorithm decreases until it reaches a minimum which is close to r_0. As time advances further, this spiral structure is destroyed by diffusion and the numerically measured radius of the smoothed-out core rises sharply with a power-law dependence on time that is identical to that of $\rho(t)$ as given by (2.13) within a time range which compares well with the spiral time range.

The anomalous behaviour given by (2.23) for times $t \ll T_S$, that is before the spiral time range, is independent of the spiral accumulation pattern. We expect to observe this scaling for initial conditions with a narrow patch. Indeed, if $r_0 = 0.6$, a move towards this behaviour can be observed and in figure 9 we compare the results for two patches of different sizes. For $r_0 = 0.3$ we also observe a decay with larger scaling exponent than $3/5$ for $t < T_S$. This behaviour can be intuitively understood as follows: if the vortex has built fine spiral structure at the inner part of the patch (and in this case the outer part is still unaffected, $t < 1$), it is again the local effect of shear that starts to destroy the structure for the very first few spiral arms before the accumulation of gradients is felt and diffusion acts according to (2.19). Thus, the observed behaviour is a weak trace of the $t^{3/2}$ decay which is asymptotically always observed for a short period of time before the spiral time range.

In §3 we demonstrated that a flow with $\Omega(r) \sim r^{-s}$ can be realized between two rotating porous cylinders. The validity of (3.18) has been checked numerically for various $Re = 3$–5. We give here a numerical example of this flow in table 4.1, and the corresponding numerical experiment is shown in figure 10.

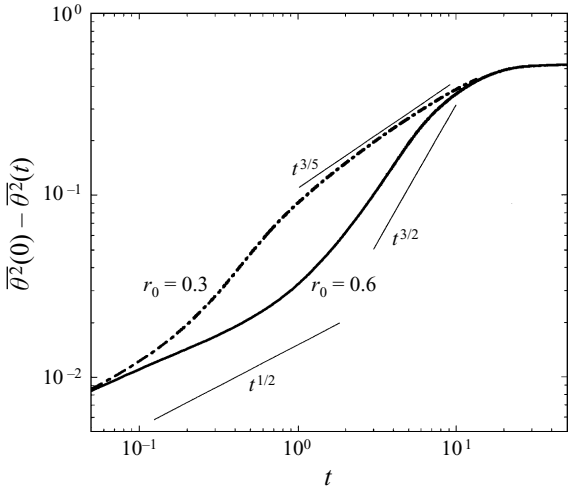

FIGURE 9. Two simulations in a vortex with $s = 4$ and different sizes of the initial scalar patch. The larger patch ($r_0 = 0.3$) decays anomalously with $\overline{\theta^2}(0) - \overline{\theta^2}(t) \sim t^{3(1-D'_K)}$, and the narrow patch ($r_0 = 0.6$) decays according to $\overline{\theta^2}(0) - \overline{\theta^2}(t) \sim t^{3/2}$.

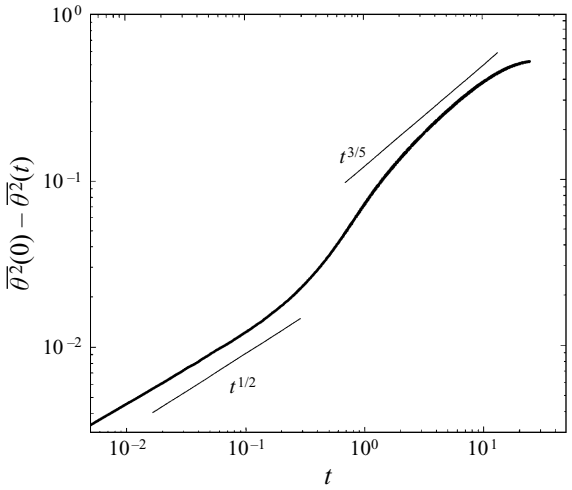

FIGURE 10. The accelerated diffusion of a scalar in the flow field between two rotating porous cylinders for the parameters of table 4.1. In the spiral time range accelerated diffusion $\overline{\theta^2}(0) - \overline{\theta^2}(t) \sim t^{3(1-D'_K)} \sim t^{3/5}$ with $D'_K = Re/(Re+1) = 4/5$ is observed.

4.2. *Kolmogorov capacities as a measure of the space-filling property of the spiral*

The vortex of the form $\Omega(r) \sim r^{-s}$ implies that at some instant t when spiral structure has formed in the scalar field, the points of discontinuity in the scalar field along a radial axis lie on $x_n = (t/n)^{1/s}$ with $n \geqslant t$. Vassilicos & Hunt (1991) showed that for such points of discontinuity $D'_K = s/(s+1)$, where D'_K is the Kolmogorov capacity or box dimension of these points.

As mentioned in the Introduction, a one-dimensional field with a spiral accumulating pattern can be alternatively described in terms of its high-wavenumber power spectrum $\Gamma(k) \sim k^{-p}$ with $p = 2 - D'_K$. In practice, the range of scales in which self-similarity can be observed is restricted. Vassilicos & Hunt (1991) showed that for

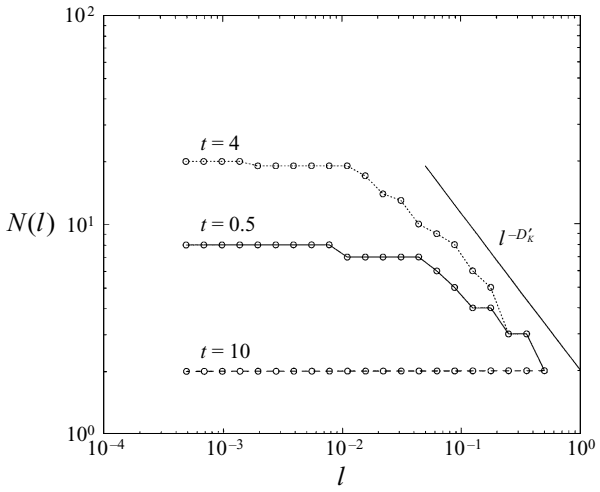

FIGURE 11. Box counting of intersections of the scalar patch along a radial line at three different times. As the vortex wraps the scalar patch into spiral structure, self-similar topology builds up ($t = 0.5, 4$) and is then rapidly wiped out ($t = 10$). The vortex scaling exponent is $s = 3$, and therefore $D'_K = 3/4$.

spiral accumulations the asymptotic value of D'_K is reached for a smaller self-similar range of scales than the range of scales needed for a clear definition of the spectral exponent p. They suggested therefore that D'_K may be a more suitable measure of self-similar geometry.

We demonstrate here that (i) the capacity D'_K is well-defined and has a constant value in the spiral time range, and that (ii) during this time range D'_K is better defined than the spectral exponent p and furthermore better defined than the dissipation power law (2.19) for the relatively low Péclet numbers that are numerically possible.

We picked as an example one numerical experiment with $s = 3$ (i.e. $D'_K = 3/4$) and measured Kolmogorov capacities and one-dimensional spectra along a radial axis at three instants of time. At $t = 0.5$ spiral structure started to build up at the centre of the vortex; at $t = 4$ the spiral expanded throughout the field; and at $t = 10$ most of the scalar was diffused. Because diffusion smooths out the initial discontinuity in the scalar field we chose thresholding to artificially restore the on–off discontinuities. The threshold value 0.5 ($\theta_0 = \{0; 1\}$) seemed to be the most sensible choice. For the spectra we additionally used running averages over a fifth of a decade to smooth the data.

In figure 11 we show the results of box counting on the scalar interface. As spiral structure builds up ($t = 0.5, 4$), a $D'_K > 0$ is observable and the range of length scales in which $D'_K > 0$ increases in time because finer and finer structure is created. At $t = 10$ diffusion has destroyed the spiral structure and as a consequence $D'_K = 0$ for all scales. These numerical results support our assumption that D'_K is independent of time within the spiral time range, an assumption that appears reasonable given the fact that we indeed find $D'_K = s/(s+1)$ for selected times in this range.

The spectra show a much weaker signature of the singularity. Isolated discontinuities result in a spectrum $\Gamma(k) \sim k^{-2}$ and this spectral slope is well observed in all three instants of time, figure 12. At $t = 4$ we observe a small range of scales in which $\Gamma(k) \sim k^{-2+D'_K}$ but we should add that the clarity of this range depends highly on

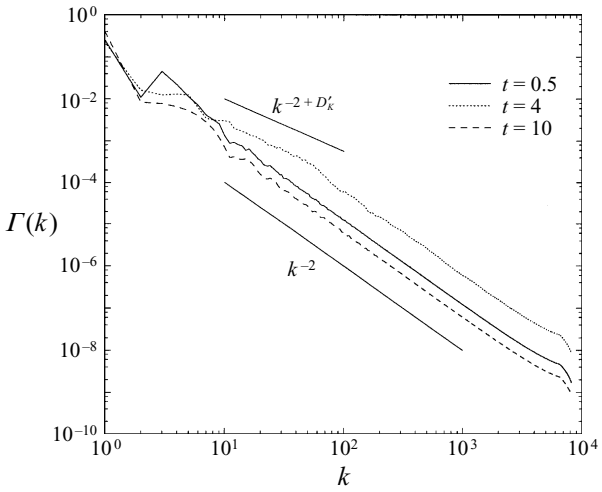

FIGURE 12. The scalar spectra of the line intersections used in figure 11. The signature of the accumulating topology, $\Gamma(k) \sim k^{-2+D'_K} = k^{-5/4}$, is only visible for $t = 4$.

the choice of running averages. Also, when using the original scalar field (without thresholding) no signature of the singularity is observed at all in the power spectrum.

To estimate D'_K from the box-counting results shown in figure 11, we compute

$$D'_K(l) = -\frac{\ln\left[N(l)/N(l_{min})\right]}{\ln\left[l/l_{min}\right]} \tag{4.1}$$

where l is the size of the covering boxes and $N(l)$ is the number of boxes needed to cover the interface. l_{min} is an inner scale which is determined by the requirement that the variance of the function $D'_K(l)$ be minimal; that is we minimize

$$\frac{1}{l_{max} - l_{min}} \int_{l_{min}}^{l_{max}} \left(D'_K(l) - \overline{D'_K}\right)^2 \mathrm{d}l \tag{4.2}$$

where

$$\overline{D'_K} = \frac{1}{l_{max} - l_{min}} \int_{l_{min}}^{l_{max}} D'_K(l)\mathrm{d}l \tag{4.3}$$

by varying l_{min} in a sub-range of $(0, l_{max}]$. The outer scale l_{max} is fixed and set as $l_{max} = R_0/2$. We set $D'_K(l) = 0$ for all $l \leqslant l_{min}$.

In figure 13 it is shown that this procedure allows D'_K to be estimated surprisingly accurately even for $t = 0.5$. The essential difference between the times $t = 0.5$ and $t = 4$ is the range over which D'_K is well-defined, the value itself is approximately constant and agrees well with the expectation $D'_K = 3/4$. Such estimates cannot be deduced from the scalar spectra. More importantly, the anomalous decay found in the numerical experiments (figure 7) allows no conclusions about the asymptotic scalar variance decay to be made because the signature is too weak for a well-defined power law in the spiral time range. However, the Kolmogorov capacity can be measured and through it (but not directly!) the prediction of the asymptotic scalar variance decay is indeed possible, even when the resolution is insufficient for the dissipation to be well-defined. Furthermore, we should also note that D'_K can easily be obtained from visualization even when the parameter s of the underlying vortex field is unknown.

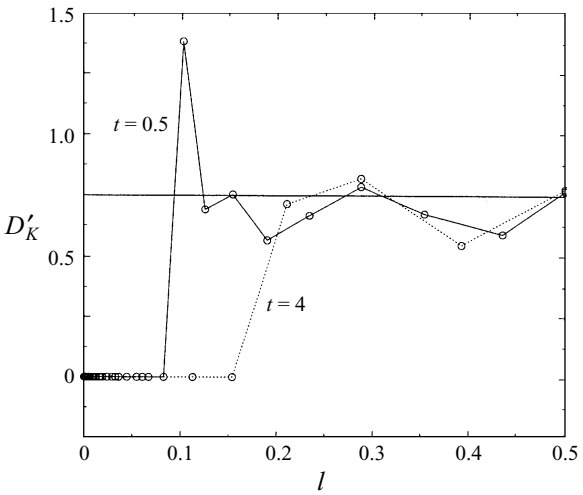

FIGURE 13. The result of estimating the Kolmogorov capacity using (4.1). The reference scale l_{min} in (4.1) is obtained from a minimizing procedure and is found to be $l_{min} = 0.1, 0.21$ for $t = 0.5, 4$.

5. Conclusions

This study was motivated by the observation that the presence of singularities in scalar fields enhances the diffusive decay of the scalar. By analysing one particular flow configuration where a spiral singularity in the scalar field is dynamically formed, it was demonstrated that the scalar dissipation is accelerated and the main result of this study is (2.19) where the accelerated diffusion is linked to the space-filling property of the spiral scalar structure.

A detailed discussion on characteristic length scales in this flow brought out the global effect of the space-filling property of the spiral accumulation of scalar gradients as opposed to the local effect that the local shear of the vortex has on the scalar patch.

In the study of turbulent flow the scalar dissipation rate is often assumed to be asymptotically independent of molecular diffusivity as mentioned in the Introduction. Here we study a specific example of a vortex flow differentially wrapping scalar around it to form a spiral structure for which

$$\chi = -\frac{\mathrm{d}}{\mathrm{d}t}\overline{\theta^2}(t) \sim \kappa^{3(1-D'_K)} t^{2-3D'_K} \tag{5.1}$$

at leading order. This implies that if $D'_K \to 1$, the dissipation χ is asymptotically independent of κ in the limit where $\kappa \to 0$, i.e. $\lim_{\kappa\to 0} \lim_{D'_K \to 1} \chi$ is a non-zero constant and independent of κ (note that these limits do not commute).

However, turbulence is perhaps not the only candidate for an application of this work; applications are to be expected wherever isolated vortices dominate the mixing properties of passive tracers like for example in atmospheric vortices which often form well-defined spiral tracer structures. The flow between rotating porous cylinders with radial suction was one particular example where we could show that the space-filling property of the scalar field which, as we show, is directly linked to the radial flow rate, accelerates scalar dissipation in a configuration that may be suitable for laboratory experiments.

A suitable measure of the space-filling property is the Kolmogorov capacity D'_K. When compared with the vortex scaling exponent s it is much easier to measure

(and visually more intuitive as it reflects the accumulating pattern of the spiral). More importantly, its value is constant over a range of times and can be accurately determined even when the resolution is too low to detect the corresponding asymptotic scaling law for the dissipation rate.

We gratefully acknowledge financial support from the Royal Society, the EPSRC (grant no. GR/K50320), the EU (contract no. ERBCHBGCT940523) and the Gottlieb Daimler- und Karl Benz-Stiftung.

Appendix. Early time asymptotics

Following the discussion in §2.2, we consider times $r_0^s \ll t \ll 1$, where only the inner part of the patch has developed spiral structure. In this time range we can distinguish between $r < t^{1/s}$, the inner part of the patch which has developed spiral structure, and $r > t^{1/s}$, the outer, unaffected part of the patch. To determine the dominant contributions in (2.9), the dependence on r and t is given by orders of magnitude:

$$\frac{\partial}{\partial t} f_n = \frac{1}{Pe}\left\{ \frac{\partial^2}{\partial r^2} f_n O(1) + \frac{\partial}{\partial r} f_n \left[O(t r^{-(s+1)}) + O(r^{-1}) \right] + f_n \left[\underbrace{O(t^2 r^{-2(s+1)})}_{\text{(i)}} + O(t r^{-(s+2)}) + \underbrace{O(r^{-2})}_{\text{(ii)}} \right] \right\}. \tag{A 1}$$

With $t < 1$ and $r < t^{1/s}$ the dominant contribution is term (i) as before. With $t < 1$ and $r > t^{1/s}$ the dominant contribution comes from the term (ii), and (2.10) becomes

$$\frac{\mathrm{d}f_n}{\mathrm{d}t} = -Pe^{-1} \left(\frac{n}{r}\right)^2 f_n \tag{A 2}$$

with the solution

$$f_n(r,t) = f_n(r,0) \exp\left[-\left(\frac{n}{r}\right)^2 Pe^{-1} t \right]. \tag{A 3}$$

This result is not surprising: the spiral part of the patch is subjected to accelerated diffusion, whereas the outer part decays according to 'classical' diffusion. Therefore, the overall decay can be written as

$$\overline{\theta^2}(0) - \overline{\theta^2}(t) \simeq \left(Pe^{-1/3} t \right)^{3(1-D'_K)} + \left(Pe^{-1} t \right)^{1/2}. \tag{A 4}$$

The first term on the right-hand side of (A 4) is dominant if spiral structure is built and destroyed faster than can be destroyed by classical diffusion, $(Pe^{-1/3}t)^{3(1-D'_K)} \gg (Pe^{-1}t)^{1/2}$. That is, anomalous decay can be observed for all $t > Pe^{(1-2D'_K)/(5-6D'_K)} = T_S^*$. Indeed $T_S^* < 1$ for $1/2 < D'_K < 5/6$, and $T_S^* < T_S$ for large Péclet numbers, that is, anomalous decay can indeed be observed for $t > T_S$ even if $T_S < 1$. For $D'_K > 5/6$ the spiral structure grows too slowly for anomalous decay to be observable for $t < 1$.

REFERENCES

Batchelor, G. K. 1959 Small-scale variation of convected quantities like temperature in turbulent fluid. Part 1. general discussion and the case of small conductivity. *J. Fluid Mech.* **5**, 113–133.

Gilbert, A. D. 1988 Spiral structures and spectra in two-dimensional turbulence. *J. Fluid Mech.* **193**, 475–497.

HUNT, J. C. R. & VASSILICOS, J. C. 1991 Kolmogorov's contributions to the physical understanding of small-scale turbulence and recent developments. *Proc. R. Soc. Lond.* A **434**, 183–210.

LUGT, H. J. 1983 *Vortex Flow in Nature and Technology*. Wiley.

MOFFATT, H. K. & KAMKAR, H. 1983 The time-scale associated with flux expulsion. In *Stellar and Planetray Magnetism* (ed. A. M. Soward), pp. 91–97. Gordon & Breach.

NIKIFORAKIS, N. & TORO, E. F. 1997 Suitability of Riemann-problem-based methods for atmospheric forced advection modelling. *UGAMP Tech. Rep. 43*. Centre for Global Atmospheric Modelling, University of Reading.

RHINES, P. B. & YOUNG, W. R. 1983 How rapidly is a passive scalar mixed within closed streamlines? *J. Fluid Mech.* **133**, 133–145.

SAFFMAN, P. 1992 *Vortex Dynamics*. Cambridge University Press.

STRANG, G. 1968 On the construction and comparison of difference schemes. *SIAM J. Numer. Anal.* **5**, 506–517.

VASSILICOS, J. C. 1995 Anomalous diffusion of isolated flow singularities and of fractal or spiral structures. *Phys. Rev.* E **52**, R1–R4.

VASSILICOS, J. C. & HUNT, J. C. R. 1991 Fractal dimensions and spectra of interfaces with application to turbulence. *Proc. R. Soc. Lond.* A **435**, 505–534.